PLACING BOUNDS ON THE NUCLEAR MATTER EQUATION OF STATE USING GRAVITATIONAL WAVE AND X-RAY OBSERVATIONS

Josef Zimmerman
Advisor: Kent Yagi

Department of Astronomy
University of Virginia
May 14, 2021

This thesis is submitted in partial completion of the requirements of the BS Astronomy-Physics Major.

Abstract

The nuclear equation of state (EoS) is poorly constrained at present. Properties of neutron stars (NSs) such as radius and tidal deformability are strongly correlated with the EoS, providing an opportunity to study nuclear matter through observations of NSs. We construct a population of EoSs by randomly sampling a multidimensional Taylor expansion, then constructing correlation distributions between the nuclear parameter $K_{\mathrm{sym},0}$, radius R, and tidal deformability Λ. Using NICER measurements of R from PSR J0030+0451 and LIGO measurements of Λ from GW170817, we develop a statistical method to place bounds on $K_{\mathrm{sym},0}$. Work is ongoing to modify the physical models for the EoS, such as the inclusion of the 3rd order symmetry parameter $J_{\mathrm{sym},0}$, which appears to produce distributions of $K_{\mathrm{sym},0}$ which are more consistent with measurements of GW170817 and J0030.

INTRODUCTION

The supranuclear equation of state (EoS), found in heavy ion collisions [1, 2] and neutron stars (NSs) [3], remains one of the biggest mysteries in nuclear physics and astrophysics to date. Macroscopic properties of an NS, such as radius and tidal deformability, are strongly dependent on the EoS relationship between energy density and pressure. This presents the opportunity to constrain the EoS using multiple measurements of independent NS observables, such as x-ray measurements of the NS mass and radius [4–8].

The historic gravitational wave (GW) detection of the merging NS binary system GW170817 [9] by the LIGO/Virgo Collaboration (LVC) presented the first opportunity to probe the interior properties of a NS through the tidal effects on the gravitational waveform [10–17]. During the inspiral, the tidal fields of each NS in the binary system induce a tidal response in the other. This effect is quantified by the *tidal deformability* parameter [18].

More recently, the Neutron Star Interior Composition Explorer (NICER), an X-ray telescope mounted on the International Space Station, performed a direct observation of the mass and radius of PSR J0030+0451 [19–24]. Using these results, many analyses have been performed to place constraints on the EoS [24–27].

In this thesis, we utilize a population of parameterized EoSs to quantify the relationship between the EoS, tidal deformability, and radius of a NS. We ultimately construct a statistical method and attempt to place bounds on the EoS utilizing the GW measurements of GW170817 and NICER measurement of J0030. This is an extension of the author's previous work placing bounds on the EoS utilizing only GW170817 [28]. This thesis is an extension of the author's previous work [29]. Throughout this thesis, we adopt the convention $G = c = 1$.

NUCLEAR MATTER PARAMETERS AND EQUATIONS OF STATE

In order to quantify properties of the EoS, we construct EoSs as a parameterized Taylor expansion, allowing correlations between nuclear parameters and NS observables to be extracted. We express the energy per nucleon $e(n, \delta)$ of supranuclear matter as a Taylor expansion in the nucleon number density n and isospin symmetry parameter $\delta \equiv (n_n - n_p)/n$ representing how neutron-richness of the matter, with n_p and n_n as the proton and neutron number densities, respectively.

The expansion goes as follows [28]. We first express $e(n, \delta)$ as the sum of the symmetric matter part $e(n, 0)$ plus the leading asymmetric part $S_2(n)$ as

$$e(n, \delta) = e(n, 0) + S_2(n)\delta^2 + \mathcal{O}(\delta^4). \tag{1}$$

We can further expand the symmetric part about nuclear saturation density n_0 using the parameters as

$$e(n, 0) = e_0 + \frac{K_0}{2}y^2 + \frac{Q_0}{6}y^3 + \mathcal{O}(y^4), \tag{2}$$

where $y \equiv (n - n_0)/3n_0$ and the coefficients represent energy per nucleon e_0, incompressibility K_0, and third derivative term Q_0, respectively. Similarly, we can expand the asymmetric part as

$$S_2(n) = J_0 + L_0 y + \frac{K_{\mathrm{sym},0}}{2}y^2 + \mathcal{O}(y^3), \tag{3}$$

where the coefficients represent symmetry energy J_0, its slope L_0, and its curvature $K_{\mathrm{sym},0}$. The lower order parameters in the expansion, such as J_0 and L_0, have been constrained with nuclear experiments [30]. On the other hand, neutron star observations can be used to measure higher order parameters like $K_{\mathrm{sym},0}$ due to their large central densities. In this thesis, we exclusively focus on placing bounds on $K_{\mathrm{sym},0}$ by combining results from GW170817 and the recent NICER measurements of the neutron star radius.

In order to maintain a model-agnostic approach and minimize systematic biases from the assumptions of EoSs motivated by microscopic physical models, we consider only EoS generated using the form of Eqs. (1)-(3). EoSs were created by randomly sampling each nuclear parameter from a uniform prior, then running tests of the physical properties of the nuclear matter and corresponding NS properties. We required that EoSs must maintain an increasing pressure p with respect to energy density ϵ as $\frac{\partial p}{\partial \epsilon} > 0$. Additionally, we require the speed of sound $c_s \equiv \sqrt{\frac{\partial p}{\partial \epsilon}} < c$ to remain causal at any central pressure p_0 below the maximum mass defined by $\frac{\mathrm{d}M}{\mathrm{d}p_0}|_{M_{max}} = 0$. Additionally, we rejected EoSs inconsistent with the 90% confidence bounds on L_0 and J_0 described in [30]. Lastly, we require that all EoSs support NSs with $M_{max} > 1.96 M_\odot$ [31]. All the EoS models considered here contain pure nuclear matter and do not contain hyperons, Bose condensates, quarks, or any other phase transition.

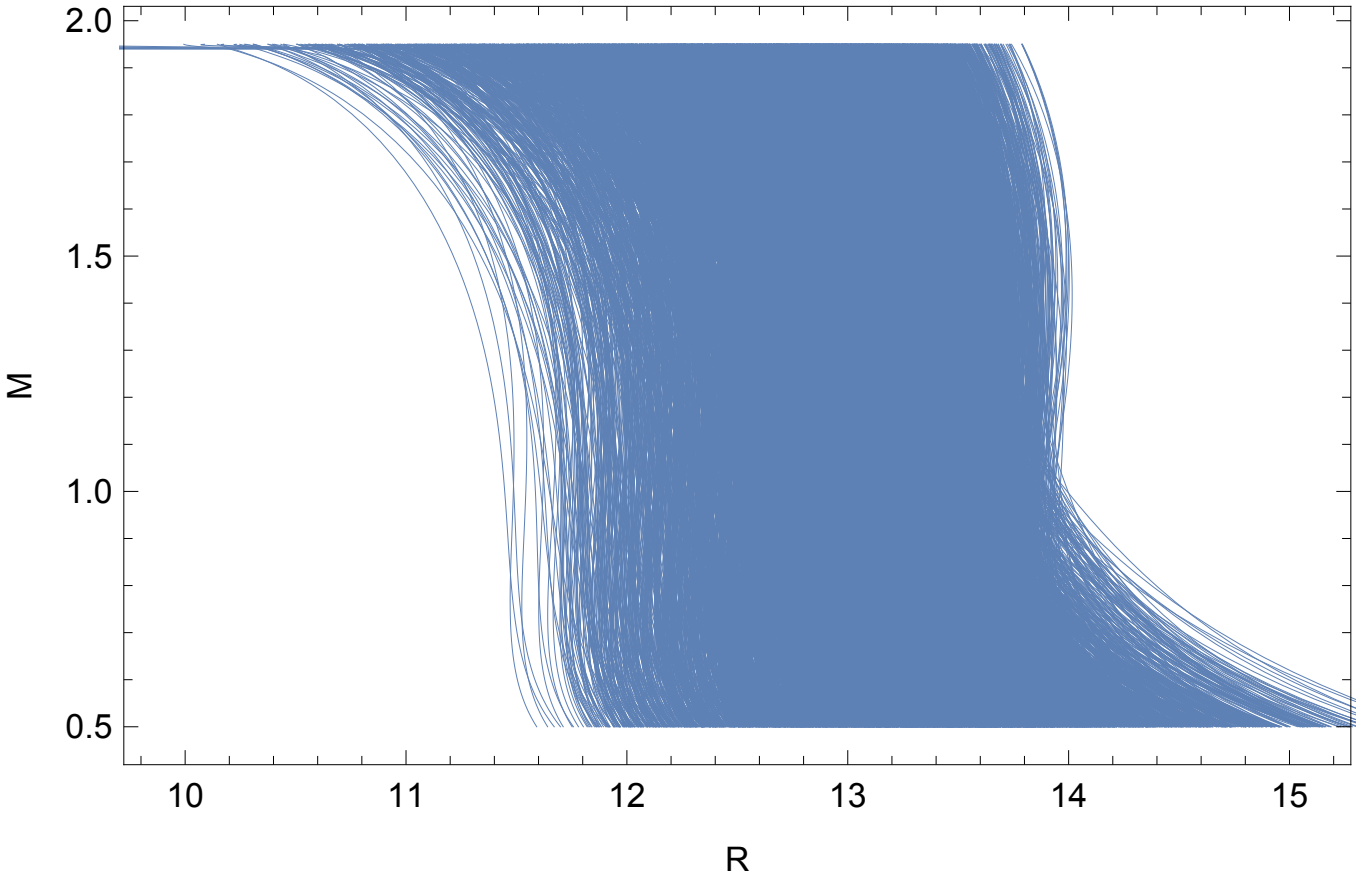

FIG. 1. Relations between the NS mass ($M_\odot$) and radius (km) for the population of EoSs. This shows that a diverse sampling regime is represented by the Taylor expansion generation of the EoS population. Acausal EoSs are included in this plot.

MASS, RADIUS AND TIDAL DEFORMABILITY

Using the population of EoSs, we compute observable NS properties, such as the mass-radius relationship and tidal deformability for each. Mass and radius are calculated by solving the Tolman-Oppenheimer-Volkhoff equations for hydrostatic equilibrium:

$$\frac{\mathrm{d}p}{\mathrm{d}r} = -\frac{(\epsilon + p)(m + 4\pi r^3 p)}{r(r - 2m)} \tag{4}$$

$$\frac{\mathrm{d}m}{\mathrm{d}r} = 4\pi\epsilon r^2, \tag{5}$$

where the EoS is used to determine ϵ as a function of p and $m(r)$ represents the gravitational mass contained within a sphere of radius r To solve Eq. (4), we pick the central pressure $p(0) \equiv p_0$ as an initial condition. We then numerically solve the differential equation until reaching the radius R where pressure vanishes $p(R) = 0$. The mass $m(R) \equiv M$ contained within that radius defines the gravitational mass of the star. Because both R and M are parameterized by p_0, we can directly relate the two variables as $R(M)$. The point where $\frac{\mathrm{d}M}{\mathrm{d}p_0} = 0$ is defined as the maximum mass M_{max} supported by the EoS.

Figure 1 shows the distribution of mass-radius curves for the EoS population, only enforcing $M_{max} > 1.96 M_\odot$, without any restrictions on the causality limit inside of the star. The figure shows a wide sampling range of masses and radii for the NS population obtained by the random sampling of nuclear parameters.

The tidal deformability λ of a NS quantifies its elasticity to develop a quadrupole moment Q_{ij} in the presence of an external tidal field $\mathcal{E}_{ij}$ as

$$Q_{ij} = -\lambda\, \mathcal{E}_{ij}. \tag{6}$$

Q_{ij} and $\mathcal{E}_{ij}$ are both obtained from the asymptotic behavior of the gravitational potential around a tidally-deformed NS. Such a stellar solution can be constructed by perturbing the non-rotating, isolated background solution derived earlier and solving a set of perturbed Einstein equations [28]. An alternative method can be used to approximate λ using the universal relations between compactness $C \equiv M/R$ and $\Lambda \equiv \lambda/M^5$ [32]:

$$\Lambda \approx 2.718^{-0.07092(-355+2.236\sqrt{4901+56400C})}. \tag{7}$$

Due to the strong coupling of tidal interaction in a binary system, it is difficult to independently measure Λ_1 and Λ_2 for each NS. Rather, we compute the mass-averaged tidal deformability

$$\tilde{\Lambda} = \frac{16}{13}\frac{(1+12q)\Lambda_1 + (12+q)q^4\Lambda_2}{(1+q)^5}, \tag{8}$$

which is the leading order tidal parameter in the gravitational waveform of a binary NS inspiral. In Eq. (8), $q \equiv m_2/m_1 < 1$ is the mass ratio and m_A and Λ_A represents the mass and dimensionless tidal deformability of the Ath neutron star respectively.

EXTRACTING CORRELATIONS

With a large population of EoSs generated and observables calculated, the next step is to construct distributions relating each relevant property of the EoS.

We begin by clarifying the role of mass in these relationships. Each nuclear parameter is determined only by the fundamental microscopic interactions of nucleons, and is thus independent of macroscopic properties of the NS such as mass. Thus, each EoS has a singular value for each parameter, including $K_{\rm sym,0}$. The NS radius, as shown in Fig 1, can vary significantly with mass. We notate the radius R associated with a particular mass M as R_M. Lastly, while Λ does vary with mass primarily due to the associated variation of radius, $\tilde{\Lambda}$ can be considered a qauntity independent of M. Previous work by the authors established that correlations between $K_{\rm sym,0}$ and $\tilde{\Lambda}$ are dominated by the chirp mass

$$\mathcal{M} \equiv \left[\frac{1}{1+q^2}\right]^{3/5}(m_1+m_2), \tag{9}$$

rather than the exact mass ratio itself [28]. Because $\mathcal{M}$ is very well constrained by GW170817, we adopt the mean values of m_1 and m_2 as measured by the LVC and ignore uncertainty in q. Thus, we obtain a singular value of $\tilde{\Lambda}_{GW170817}$[1] predicted by each EoS that should have been observed in GW170817, independent of any mass uncertainty.

Because the population of EoSs provides only discrete points, we must interpolate to produce a continuous distribution. We use binning and interpolation to produce a continuous distribution $P(K_{\rm sym,0}, R_M, \tilde{\Lambda}_{GW170817})$ between R_M, $\tilde{\Lambda}_{GW170817}$ and $K_{\rm sym,0}$, rather than assuming a Gaussian relationship as in previous work. [28].

Finally, we must normalize the relationships as conditional probability distributions on R_M and $\tilde{\Lambda}_{GW170817}$, performed as

$$P(K_{\rm sym,0}|R_M, \tilde{\Lambda}_{GW170817}) = \frac{P(K_{\rm sym,0}, R_M, \tilde{\Lambda}_{GW170817})}{\int_{-\infty}^{\infty} P(K'_{\rm sym,0}, R_M, \tilde{\Lambda}_{GW170817}) \mathrm{d}K'_{\rm sym,0}}. \tag{10}$$

BOUNDS ON $K_{\rm sym,0}$ FROM NICER

We now describe the process to derive bounds on $K_{\rm sym,0}$ from the NICER's measurement of the NS mass and radius for PSR J0030+0451. We explore the results of the NICER study [20], released as the Markov Chain Monte Carlo (MCMC) samples for pairs of mass and radius measured from the NS. Because of the strong degeneracy between mass and radius in the NICER posterior measurement, our statistical procedures must account for uncertainty in mass. We accomplish this by constructing bins of nearly constant mass from the NICER posterior. This is performed such

[1] We denote the measurement of $\tilde{\Lambda}$ with the subscript GW170817 to emphasize that is a measurement unique to the exact combination of NS masses involved in the event

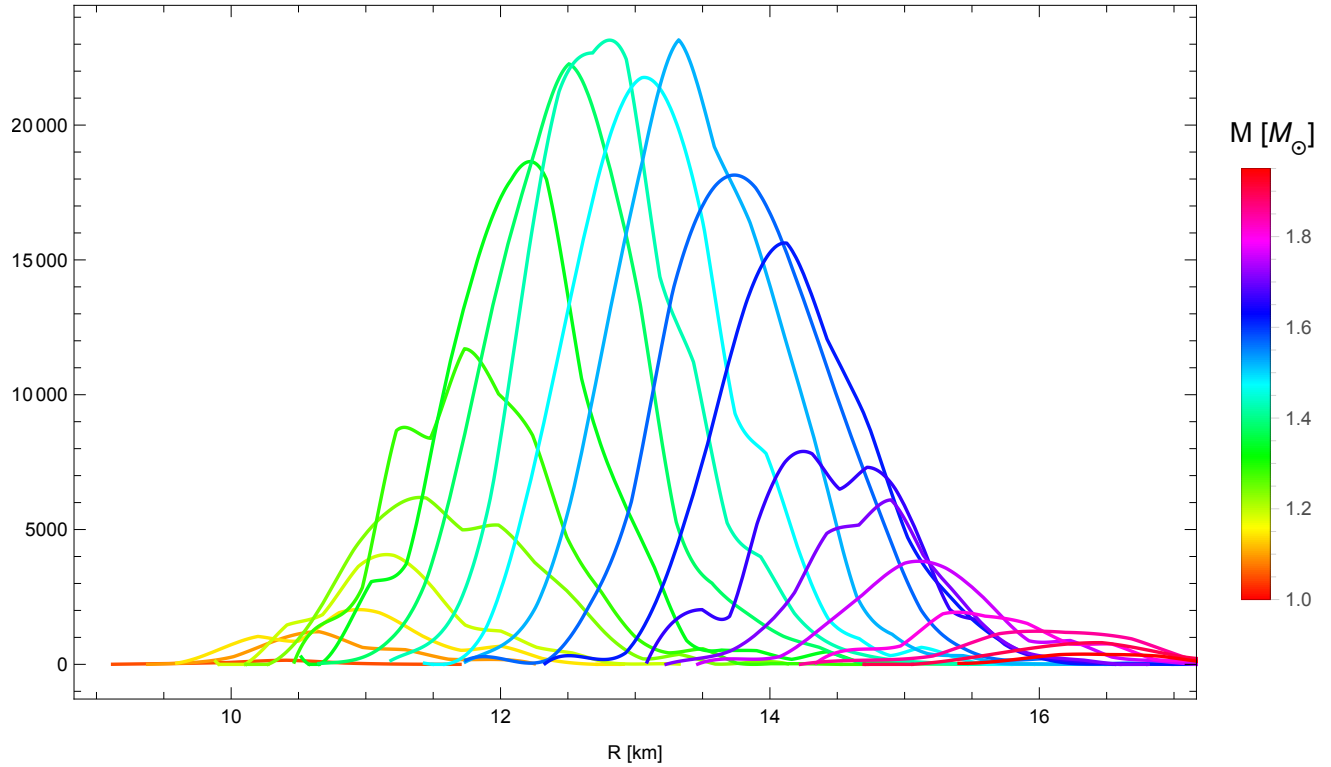

FIG. 2. 20 mass bins, each with a width of 0.05 $M_\odot$ divide the NICER measurement into approximations for $P(R_M)$ with small uncertainty in m relative to the statistical spread of R_M. Added together, the 20 distributions for $P(R_M)$ reconstruct the original NICER measurement by Miller et Al.[20]

that the statistical uncertainty of radius R_M samples falling within that bin is much greater than the difference in average radius measurement between different mass bins $\Delta\overline{R}_m \equiv \overline{R}_{(m+\delta)} - \overline{R}_m$. We first divide NICER's results into 20 bins of mass evenly spaced between 1 and 1.95 $M_\odot$[2]. The MCMC samples within each mass bin that starts with mass M give us the probability distribution of the radius samples at that fixed mass M. The samples of R that fall within the bin allow us to construct one-dimensional posterior approximations for $P(R_M)$, which are shown in Fig 2 to reconstruct the entire distribution by Miller et Al. [20].

By converting the J0030 measurements into a series of measurements binned by nearly definite mass, we match the conditional probability distributions obtained from the EoS population, which only permit a measurement of radius given a definite mass, rather than a correlated uncertainty between the two quantities. One such distribution is shown in Fig 3, which suggests that more positive values of $K_{\rm sym,0}$ are consistent with the data. This is inconsistent with past measurements of $K_{\rm sym,0}$, which generally find $K_{\rm sym,0} \lesssim 0$ [33, 34]. Additionally, part of the distribution for $P(R_M)$ extends beyond the range of radii observed in the simulated EoS population, indicating that our population may be inconsistent with the NICER measurements.

The final step is to attempt to place probabilistic bounds on $K_{\rm sym,0}$ using a combination of the observed data and simulated correlations, which is achieved using marginalization integrals. Using only the NICER X-ray measurements, the probability distribution of $K_{\rm sym,0}$ from one mass bin at M is given by

$$P_{\rm M}(K_{\rm sym,0}) = \int_{-\infty}^{\infty} P_{\rm M}(K_{\rm sym,0}|R_{\rm M})\, P(R_{\rm M})\, dR_{\rm M}. \tag{11}$$

where $P_{\rm M}(K_{\rm sym,0}|R_{\rm M})$ is the two-dimensional conditional probability distribution corresponding to Eq. (10). This way, we can take into account the amount of scattering in the correlation between $K_{\rm sym,0}$ and $R_{\rm M}$, which adds a systematic error to the final distribution on $K_{\rm sym,0}$. After normalizing it properly, this yields bounds on $K_{\rm sym,0}$ for

[2] We have checked that when we increase the number of bins to 40, the final bound on $K_{\rm sym,0}$ only changed by less than 1 MeV.

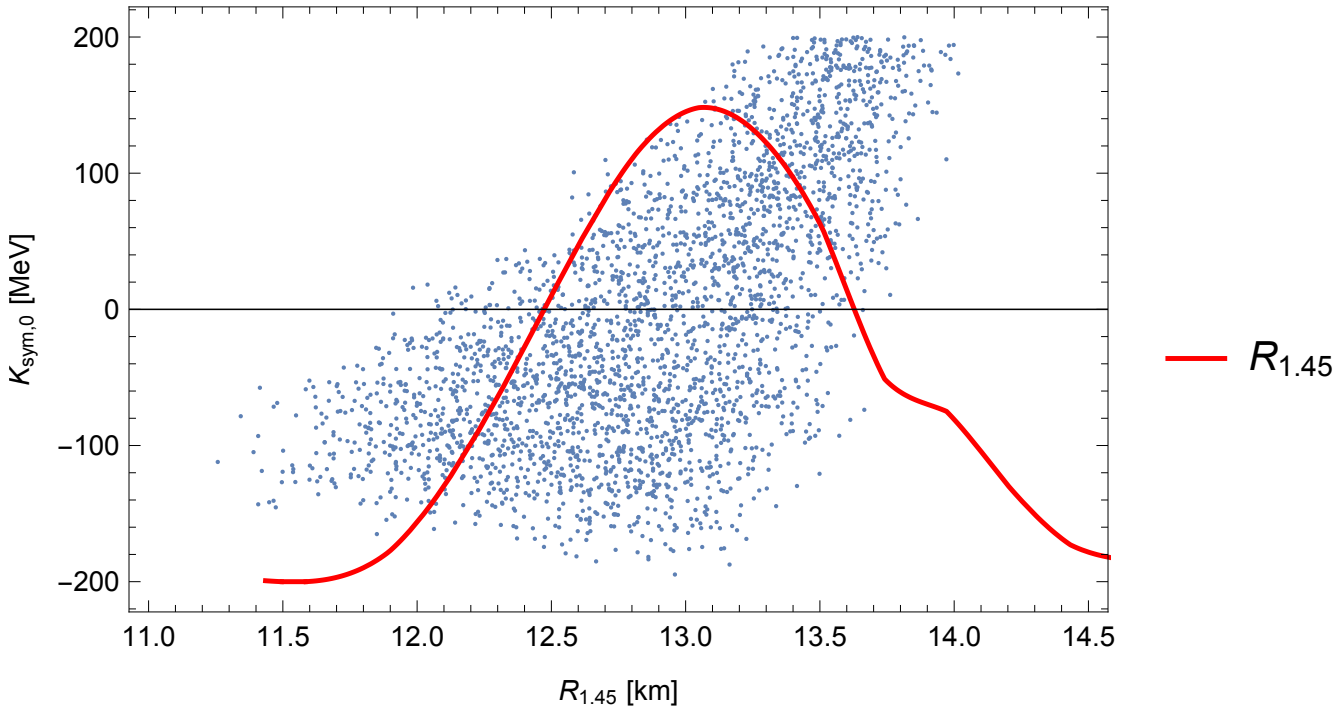

FIG. 3. A single mass bin for $R_{1.45}$ is shown, with the scatter plot distribution for $P(K_{\rm sym,0}, R_1.45)$ and the NICER measurement for $P(R_{1.45})$. The distributions favor more positive values of $K_{\rm sym,0}$, and even extend to slightly larger radii than were consistent with the results from EoS population synthesis.

each fixed value of mass M. The final step combines each bound weighted by the probability distribution of the mass $P(M)$ constructed from the number of NICER samples in each mass bin:

$$P(K_{\rm sym,0}) = \sum P_{\rm M}(K_{\rm sym,0}) P(M). \tag{12}$$

Due to the misalignment between $P(R_M)$ and $P_m(K_{\rm sym,0}, R_M)$, the marginalization calculation does not yield reasonable bounds. The final bounds on $K_{\rm sym,0}$ are constrained by the prior uniform sampling limit of $K_{\rm sym,0} < 200$ MeV. For example, previous bounds of $K_{\rm sym,0} = -125 \pm 79$ MeV [33] and $K_{\rm sym,0} = -230^{+90}_{-50}$ MeV [34] are both constrained well below our 200 MeV limit. Even accounting for differences in assumptions, this inconsistency is not explainable statistically.

One possible resolution to the inconsistent bounds on $K_{\rm sym,0}$ may be to include a secondary constraint from the LVC measurement of GW170817. Because the NICER measurement favors larger values of $K_{\rm sym,0}$, the GW170817 measurement's relatively negative bounds on $K_{\rm sym,0}$ may taper the outlying probabilities [28]. We use the three-dimensional probability distribution $P_{\rm M}(K_{\rm sym,0}|R_{\rm M}, \tilde{\Lambda}_{GW170817})$ from Eq. (10) relating $K_{\rm sym,0}$, $R_{\rm M}$ and $\tilde{\Lambda}_{GW170817}$. We can first use the tidal measurement of $P(\tilde{\Lambda}_{GW170817})$ by the LVC [35] to marginalize the above three-dimensional probability distribution over $\tilde{\Lambda}_{GW170817}$ to obtain $P_{\rm M}(K_{\rm sym,0}, R_{\rm M})$:

$$P_{\rm M}(K_{\rm sym,0}|R_{\rm M}) = \int_{-\infty}^{\infty} P_{\rm M}(K_{\rm sym,0}|R_{\rm M}, \tilde{\Lambda}_{GW170817}) \times P(\tilde{\Lambda}_{GW170817})\, {\rm d}\tilde{\Lambda}_{GW170817}. \tag{13}$$

We then proceed according to Eqs. (11) and (12) to obtain final bounds on $K_{\rm sym,0}$. Research is ongoing to compute this statistical bound using numerical methods properly and ensure that the final bounds are statistically reasonable. The presently calculated distribution between $K_{\rm sym,0}$ and $\tilde{\Lambda}_{GW170817}$, shown in Fig 4 also appears inconsistent with the measurement of GW170817 in the small $K_{\rm sym,0}$ region. This finding is inconsistent with the past investigation of $\tilde{\Lambda}$ and $K_{\rm sym,0}$ using randomly sampled EoSs [28].

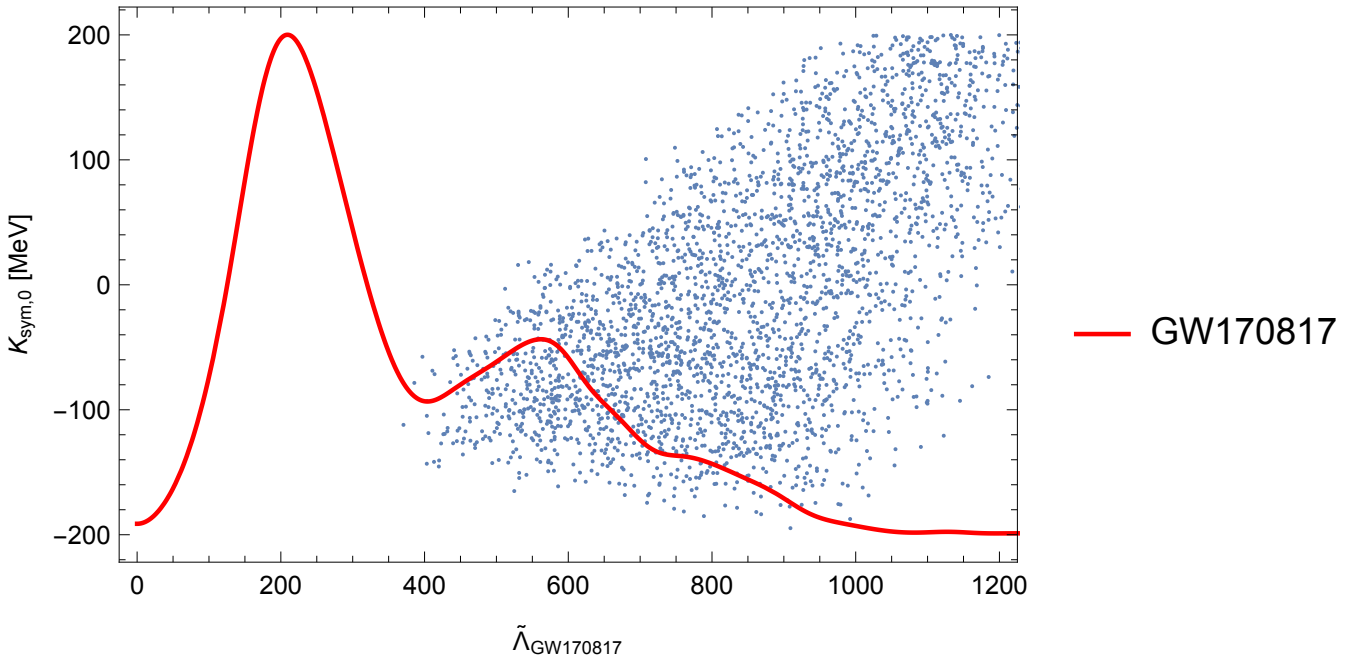

FIG. 4. The LVC measurement of $\tilde{\Lambda}$ for GW170817 is inconsistent with the population of EoSs, which do not display values below 400.

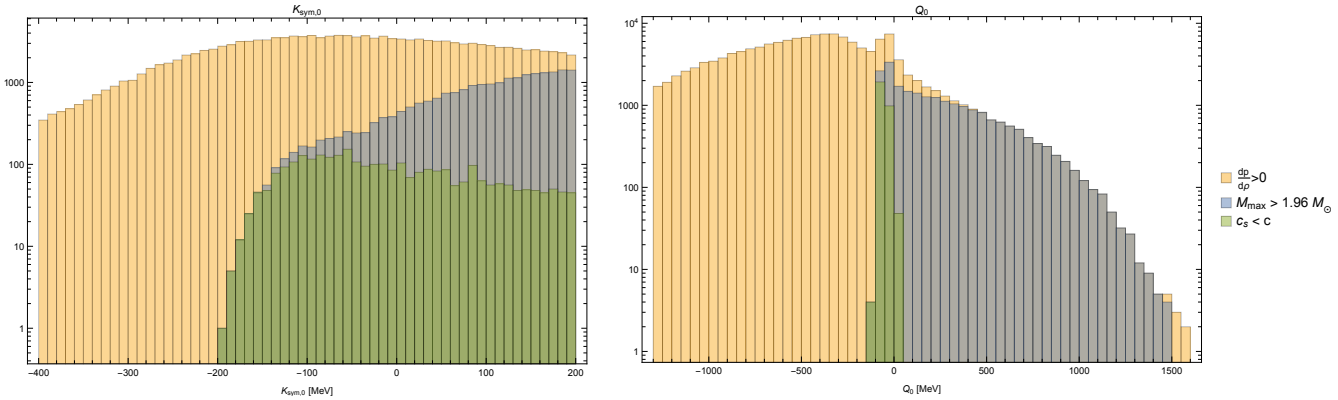

FIG. 5. This logarithmic histogram shows the distributions of $K_{\rm sym,0}$ and Q_0 for the EoS population after various physicality requirements have been applied in succession. Beginning from a uniform distribution of $K_{\rm sym,0}$ and Q_0 samples, the first requirement $\frac{dp}{d\epsilon} > 0$ requires that pressure must increase monotonically. The next requirement $M_{max} > 1.96 M_\odot$ ensures EoSs are able to reproduce the 2σ lower bound of the mass of J0740 [31], which strongly favors larger values of $K_{\rm sym,0}$ and Q_0. Lastly, the final requirement $c_s < c$ ensures the speed of sound inside the nuclear matter remains causal, which slightly favors lower values of $K_{\rm sym,0}$, but very strongly constrains the range of Q_0.

INVESTIGATION OF INCONSISTENCIES

We have seen that the Taylor expansion-generated EoS population is unable to reproduce the range of measurements of R by NICER, nor the range of probable $\tilde{\Lambda}_{GW170817}$ by LIGO/Virgo. While it is possible an error exists in our analysis, we have conducted thorough review of each step in the process and all but excluded that possibility. Rather, we believe that the source of inconsistency lies in the choice to use $K_{\rm sym,0}$ as the highest order parameter in the expansion of Eq. (3).

In the work of Carson et Al., the phenomenologically sampled EoSs were not required to respect causality with $c_s < c$ [28]. While Fig 5 shows that the causality requirement changes the distribution of $K_{\rm sym,0}$ samples, the dominant effect of the causality requirement is on the 3rd order parameter Q_0 in Eq (2). Whereas Carson et Al. included EoSs

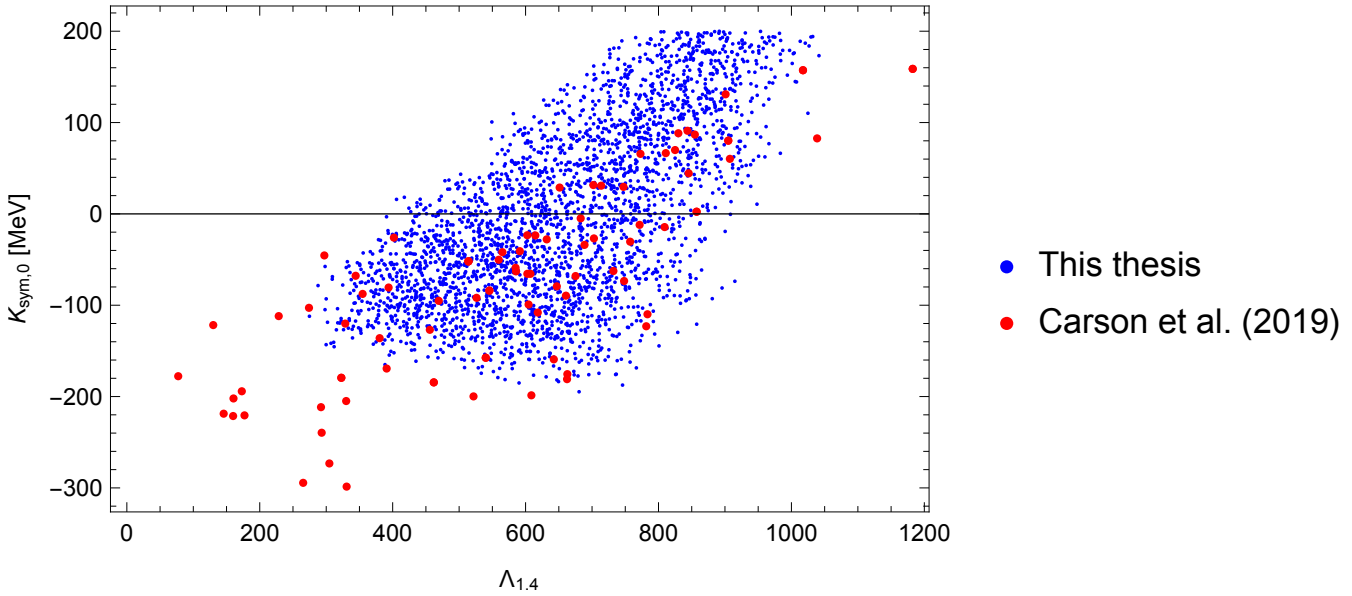

FIG. 6. The $K_{\rm sym,0}$ and $\Lambda_{1.4}$ distributions are compared for this thesis and Carson et al. [28]. Blue shows the main method of this analysis, utilizing the universal relation of Eq. (7) to approximate Λ from C. Red points show the phenomenological EoSs of Carson et Al., which extend to much lower values of $K_{\rm sym,0}$ and $\Lambda_{1.4}$ than are represented in the aforementioned distribution.

with Q_0 as large as 1500 MeV, we find that by enforcing the causality requirement, $Q_0 < 15$ MeV.

This finding is expected, as c_s generally— although not strictly—increases with increasing pressure. Because c_s is evaluated at the maximum possible NS mass M_{max} for a given EoS, which corresponds to the greatest stable pressure possible under the EoS, this condition corresponds to extremely large energy densities. Because the 3rd order parameter Q_0 dominates over the 2nd order $K_{\rm sym,0}$ at densities much greater than saturation density, Q_0 is more strongly limited by the causality restriction than $K_{\rm sym,0}$. Similar logic follows for the M_{max} requirement, which as shown in Fig 5 produces a sharper cutoff for the lower end of the Q_0 distribution than the $K_{\rm sym,0}$ distribution.

We can use this analysis of the $K_{\rm sym,0}$ and Q_0 distributions to motivate a potential solution to the inconsistency between our theoretical models of R and $\tilde{\Lambda}$ and the NS measurements from NICER and LIGO/Virgo.

Comparing the distribution of $K_{\rm sym,0}$ and $\Lambda_{1.4}$ for three different methods, we can search for errors in our analysis and compare to the past work of Carson et Al. [28]. Figure 6 shows this distribution as calculated using the universal relation in Eq. (7), directly using a TOV solution to quadrupolar perturbation (see Carson et Al. for a detailed description of this method), and lastly the original results of Carson et Al. [28]. Although there is some expected inconsistency between the universal relation and TOV calculation of $\Lambda_{1.4}$ because they are preformed on similar—but not identical—population of EoSs, there appears to be a non-statistical inconsistency at large values of $\Lambda_{1.4}$; this is due to numerical errors in the TOV solver for NSs with large deformability and is not a real inconsistency. However, there is a true inconsistency with the distribution of Carson et Al, which features much lower samples of $K_{\rm sym,0}$ and $\Lambda_{1.4}$ than our analysis. Upon inspecting the EoSs of Carson et Al, we found that the EoSs in question corresponded to very large values of Q_0, and thus would have been rejected by our causality restriction.

MODELLING OF $J_{\rm sym,0}$

Ultimately, we must produce a population of EoSs including these very negative values of $K_{\rm sym,0}$, which as shown clearly in Fig 6 will correspond to the missing small values of Λ, and similarly to the small $\tilde{\Lambda}$ missing from Fig. 4. As we have shown in Fig. 5 that enforcing the causality and maximum mass requirements most strongly restricts the highest order parameter, we propose modifying the Taylor expansion model in Eq. (3) to include the 3rd order symmetry energy parameter $J_{\rm sym,0}$:

$$S_2(n) = J_0 + L_0 y + \frac{K_{\rm sym,0}}{2} y^2 + \frac{J_{\rm sym,0}}{6} y^3 + \mathcal{O}(y^4). \tag{14}$$

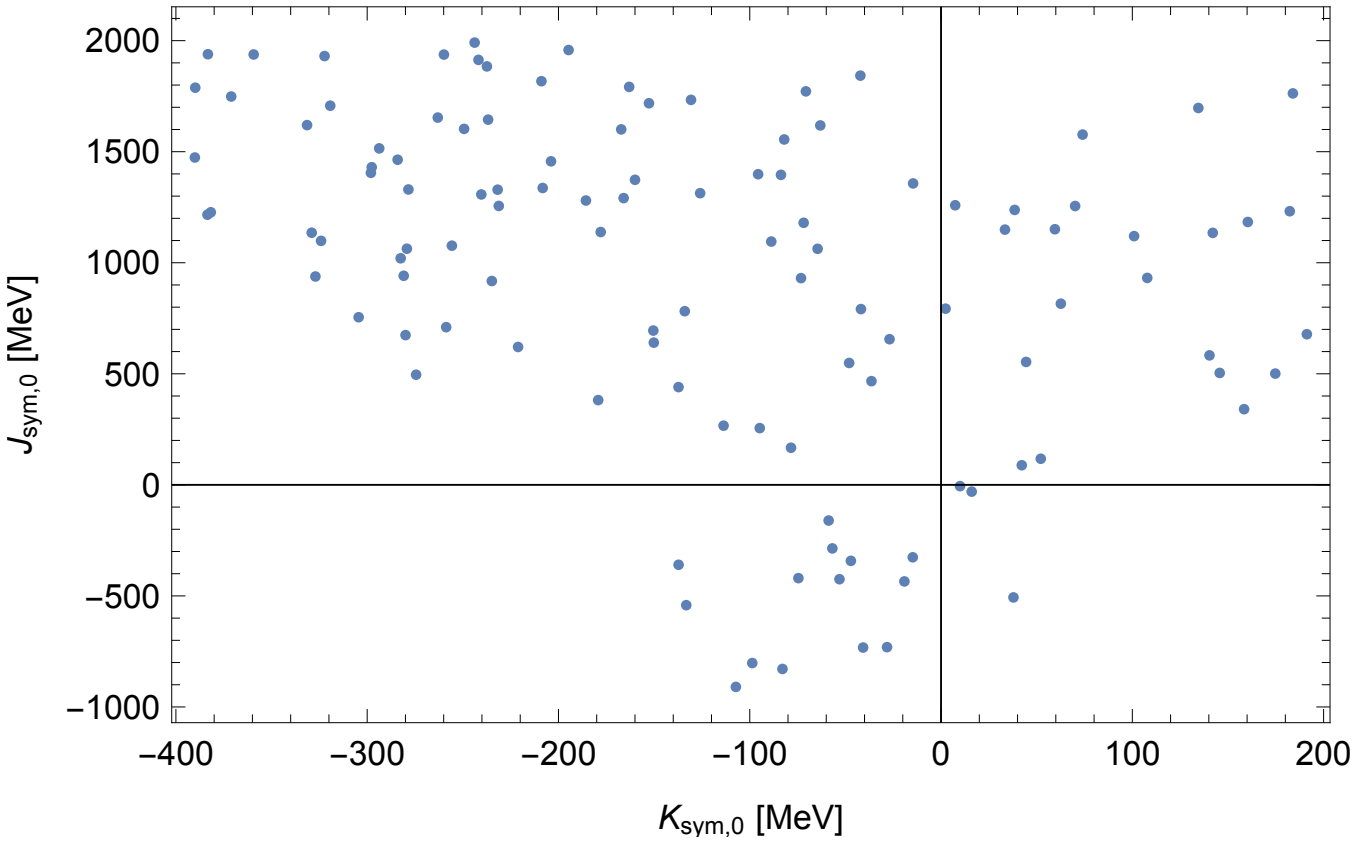

FIG. 7. A sample of ~ 115 EoSs with varying $J_{\rm sym,0}$ shows the correlations between $K_{\rm sym,0}$ and $J_{\rm sym,0}$. By allowing $J_{\rm sym,0}$ to increase, EoSs with smaller values of $K_{\rm sym,0}$ still achieve a maximum mass $M_{max} > 1.96 M_\odot$, thus producing a wider range of valid $K_{\rm sym,0}$ values.

Beyond simply matching the 3rd order form of Eq. (2), $J_{\rm sym,0}$ will dominate over $K_{\rm sym,0}$ in the EoS at extremely high densities. Whereas the missing low values of $K_{\rm sym,0}$ are presently rejected by the M_{max} requirement, we expect that this requirement will more strongly limit the distribution of $J_{\rm sym,0}$ and instead allow smaller values of $K_{\rm sym,0}$ to be obtained without decreasing M_{max}. Past studies have found that the inclusion of $J_{\rm sym,0}$ produced more negative bounds on $K_{\rm sym,0}$ [36]. We emphasize that $J_{\rm sym,0}$ was not necessary in Carson et Al. because, by not enforcing causality in the NS interior, the large values of Q_0 supported large NS masses and allowed more freedom in $K_{\rm sym,0}$.

A small sample population of EoSs was generated with a randomly sampled range of -1000 MeV $< J_{\rm sym,0} <$ 2000 MeV. While this small number of EoSs is insufficient to test the statistical bounds on $K_{\rm sym,0}$ using measurements extracted from GW170817 and J0030, the preliminary distributions provide insight through comparison with the original $J_{\rm sym,0} = 0$ population.

First, we can compare how the distribution of $K_{\rm sym,0}$ changes with the introduction of a varying $J_{\rm sym,0}$, illustrated in Fig. 7. By allowing $J_{\rm sym,0}$ to reach large values, EoSs with smaller values of $K_{\rm sym,0}$ satisfy the $M_{max} > 1.96 M_\odot$ requirement and remain physically viable. While the sampling is currently very sparse, there appears to be a roughly linear cutoff to the minimum $K_{\rm sym,0}$ permitted given a value of $J_{\rm sym,0}$, shown in Fig. 7 as the boundary between the region in the lower-left corner of the plot without any EoSs and the remainder of the EoS distribution.

Additionally, we can inspect the preliminary distribution between $K_{\rm sym,0}$ and $\tilde{\Lambda}_{\rm GW170817}$, shown in Fig. 8. Because varying $J_{\rm sym,0}$ produced lower values of $K_{\rm sym,0}$ and the lower values of $K_{\rm sym,0}$ generally correspond to smaller deformability, the new distribution is slightly more consistent with the GW170817 event than the fixed $J_{\rm sym,0} = 0$ case. The new distribution produces EoSs with $\tilde{\Lambda}_{\rm GW170817} \sim 275$, compared to a minimum of ~ 400 in the $J_{\rm sym,0} = 0$ distribution. This is expected to produce more reliable bounds on $K_{\rm sym,0}$ using the GW170817 event than previously obtainable.

Because the preliminary results for varying $J_{\rm sym,0}$ appear promising, a much larger EoS population will be generated using this method. Once a larger population is created, the correlation between $K_{\rm sym,0}$ and $\tilde{\Lambda}_{\rm GW170817}$ can be converted to a continuous distribution as described previously. This will ultimately allow bounds on $K_{\rm sym,0}$ to be produced once

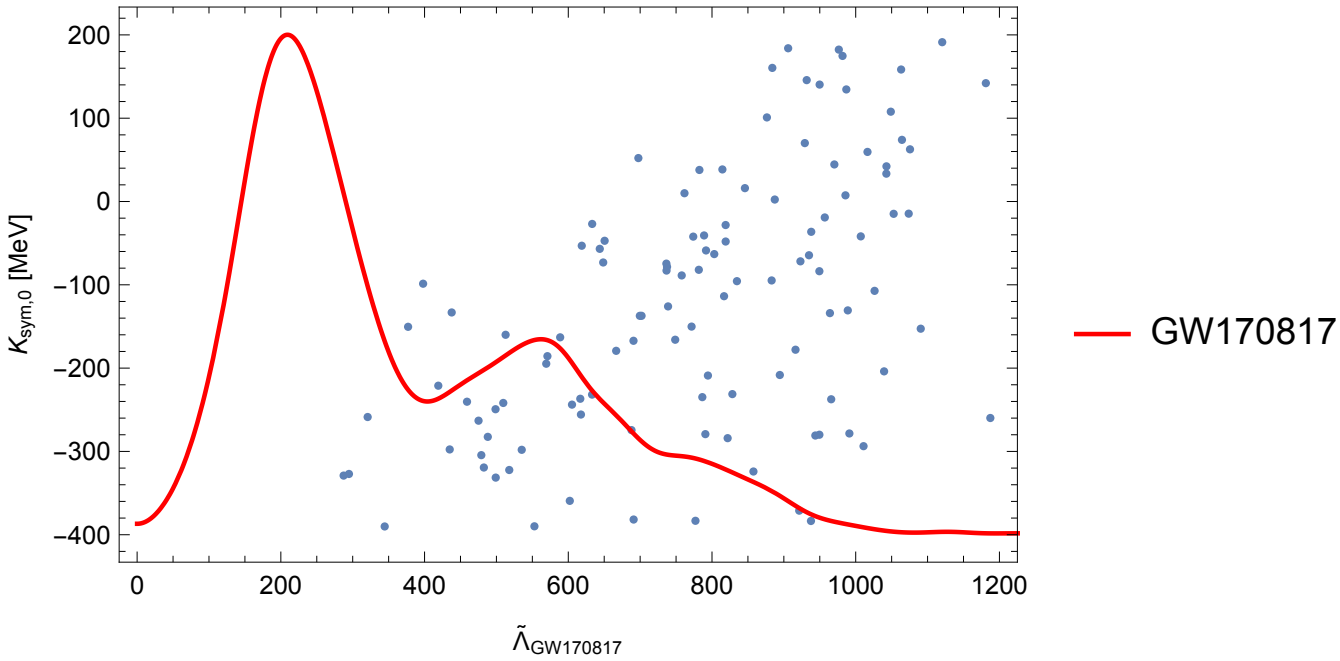

FIG. 8. By including a randomly sampled $J_{\rm sym,0}$ parameter, the EoS population includes samples with $\tilde{\Lambda}_{\rm GW170817} \sim 275$, which is significantly lower than the fixed $J_{\rm sym,0} = 0$ case, which only produces a lower limit of $\tilde{\Lambda}_{\rm GW170817} \sim 400$, shown in Fig. 4. While still inconsistent with the measurement of $\tilde{\Lambda}_{\rm GW170817}$, the inconsistency is smaller, and an increase to the sampling range of $J_{\rm sym,0}$ is likely to allow the production of less deformable EoSs.

a large enough population of EoSs is generated. Work on this subject will continue during the summer, with the goal to produce reliable bounds on $K_{\rm sym,0}$.

CONCLUSIONS AND DISCUSSIONS

We constructed a large population of randomly sampled Taylor expanded EoSs, quantifying the relationships between the nuclear parameter $K_{\rm sym,0}$ and the physical observables R and $\tilde{\Lambda}$. By constructing multidimensional conditional probability distributions, we designed a statistical process that can place bounds on $K_{\rm sym,0}$ given a measurement of radius and tidal deformability of a NS. While complications have prevented reliable bounds on $K_{\rm sym,0}$ from being obtained thus far, work is continuing to produce reasonable constraints on the EoS.

The EoS models have been modified to include a varying $J_{\rm sym,0}$. While it is unlikely to be directly measurable using the current data sets, its inclusion appears to shift the distribution of $K_{\rm sym,0}$ in such a way that it corresponds more closely with the measurement of GW170817, producing more reliable bounds on $K_{\rm sym,0}$.

Future work will modify the statistical procedures of this project to incorporate the NICER measurement of the pulsar J0740. Although its large mass will provide some complications for Taylor expansion EoSs, which become less accurate at higher energy densities due to the omission of higher order parameters beyond Q_0 and $J_{\rm sym,0}$, it is still likely to produce additional constraints on $K_{\rm sym,0}$.

Acknowledgments— J.Z. was supported by the Virginia Space Grant Consortium.

[1] P. Danielewicz, R. Lacey, and W. G. Lynch, Science **298**, 1592 (2002), arXiv:nucl-th/0208016 [nucl-th].
[2] M. Tsang, Y. Zhang, P. Danielewicz, M. Famiano, Z. Li, W. Lynch, and A. Steiner, Phys.Rev.Lett. **102**, 122701 (2009), arXiv:0811.3107 [nucl-ex].
[3] J. Lattimer and M. Prakash, Astrophys.J. **550**, 426 (2001), arXiv:astro-ph/0002232.

[4] T. Guver and F. Ozel, Astrophys. J. **765**, L1 (2013), arXiv:1301.0831 [astro-ph.HE].
[5] F. Ozel, G. Baym, and T. Guver, Phys.Rev. **D82**, 101301 (2010), arXiv:1002.3153 [astro-ph.HE].
[6] A. W. Steiner, J. M. Lattimer, and E. F. Brown, Astrophys.J. **722**, 33 (2010).
[7] J. M. Lattimer and A. W. Steiner, The European Physical Journal A **50** (2014), 10.1140/epja/i2014-14040-y.
[8] F. Ozel and P. Freire, Ann. Rev. Astron. Astrophys. **54**, 401 (2016), arXiv:1603.02698 [astro-ph.HE].
[9] B. P. Abbott *et al.* (Virgo, LIGO Scientific), Phys. Rev. Lett. **119**, 161101 (2017), arXiv:1710.05832 [gr-qc].
[10] B. P. Abbott *et al.* (LIGO Scientific, Virgo), Phys. Rev. **X9**, 011001 (2019), arXiv:1805.11579 [gr-qc].
[11] B. P. Abbott *et al.* (LIGO Scientific, Virgo), Phys. Rev. Lett. **121**, 161101 (2018), arXiv:1805.11581 [gr-qc].
[12] V. Paschalidis, K. Yagi, D. Alvarez-Castillo, D. B. Blaschke, and A. Sedrakian, Physical Review D **97** (2018), 10.1103/physrevd.97.084038.
[13] G. F. Burgio, A. Drago, G. Pagliara, H. J. Schulze, and J. B. Wei, Arxiv (2018), 1803.09696v1.
[14] T. Malik, N. Alam, M. Fortin, C. Providência, B. K. Agrawal, T. K. Jha, B. Kumar, and S. K. Patra, Phys. Rev. **C98**, 035804 (2018), arXiv:1805.11963 [nucl-th].
[15] P. Landry and R. Essick, Phys. Rev. **D99**, 084049 (2019), arXiv:1811.12529 [gr-qc].
[16] L. Baiotti, Prog. Part. Nucl. Phys. **109**, 103714 (2019), arXiv:1907.08534 [astro-ph.HE].
[17] A. Guerra Chaves and T. Hinderer, J. Phys. **G46**, 123002 (2019), arXiv:1912.01461 [nucl-th].
[18] É. É. Flanagan and T. Hinderer, Physical Review D **77** (2008), 10.1103/physrevd.77.021502.
[19] T. E. Riley, A. L. Watts, S. Bogdanov, P. S. Ray, R. M. Ludlam, S. Guillot, Z. Arzoumanian, C. L. Baker, A. V. Bilous, D. Chakrabarty, K. C. Gendreau, A. K. Harding, W. C. G. Ho, J. M. Lattimer, S. M. Morsink, and T. E. Strohmayer, The Astrophysical Journal **887**, L21 (2019).
[20] M. C. Miller, F. K. Lamb, A. J. Dittmann, S. Bogdanov, Z. Arzoumanian, K. C. Gendreau, S. Guillot, A. K. Harding, W. C. G. Ho, J. M. Lattimer, R. M. Ludlam, S. Mahmoodifar, S. M. Morsink, P. S. Ray, T. E. Strohmayer, K. S. Wood, T. Enoto, R. Foster, T. Okajima, G. Prigozhin, and Y. Soong, The Astrophysical Journal **887**, L24 (2019).
[21] S. Bogdanov, S. Guillot, P. S. Ray, M. T. Wolff, D. Chakrabarty, W. C. G. Ho, M. Kerr, F. K. Lamb, A. Lommen, R. M. Ludlam, R. Milburn, S. Montano, M. C. Miller, M. Bauböck, F. Özel, D. Psaltis, R. A. Remillard, T. E. Riley, J. F. Steiner, T. E. Strohmayer, A. L. Watts, K. S. Wood, J. Zeldes, T. Enoto, T. Okajima, J. W. Kellogg, C. Baker, C. B. Markwardt, Z. Arzoumanian, and K. C. Gendreau, The Astrophysical Journal **887**, L25 (2019).
[22] S. Bogdanov, F. K. Lamb, S. Mahmoodifar, M. C. Miller, S. M. Morsink, T. E. Riley, T. E. Strohmayer, A. K. Tung, A. L. Watts, A. J. Dittmann, D. Chakrabarty, S. Guillot, Z. Arzoumanian, and K. C. Gendreau, The Astrophysical Journal **887**, L26 (2019).
[23] S. Guillot, M. Kerr, P. S. Ray, S. Bogdanov, S. Ransom, J. S. Deneva, Z. Arzoumanian, P. Bult, D. Chakrabarty, K. C. Gendreau, W. C. G. Ho, G. K. Jaisawal, C. Malacaria, M. C. Miller, T. E. Strohmayer, M. T. Wolff, K. S. Wood, N. A. Webb, L. Guillemot, I. Cognard, and G. Theureau, The Astrophysical Journal **887**, L27 (2019).
[24] G. Raaijmakers, T. E. Riley, A. L. Watts, S. K. Greif, S. M. Morsink, K. Hebeler, A. Schwenk, T. Hinderer, S. Nissanke, S. Guillot, Z. Arzoumanian, S. Bogdanov, D. Chakrabarty, K. C. Gendreau, W. C. G. Ho, J. M. Lattimer, R. M. Ludlam, and M. T. Wolff, The Astrophysical Journal **887**, L22 (2019).
[25] J.-E. Christian and J. Schaffner-Bielich, (2019), arXiv:1912.09809 [astro-ph.HE].
[26] J.-L. Jiang, S.-P. Tang, Y.-Z. Wang, Y.-Z. Fan, and D.-M. Wei, (2019), arXiv:1912.07467 [astro-ph.HE].
[27] G. Raaijmakers *et al.*, (2019), arXiv:1912.11031 [astro-ph.HE].
[28] Z. Carson, A. W. Steiner, and K. Yagi, Phys. Rev. D **99**, 043010 (2019).
[29] J. Zimmerman, Z. Carson, K. Schumacher, A. W. Steiner, and K. Yagi, arXiv e-prints , arXiv:2002.03210 (2020), arXiv:2002.03210 [astro-ph.HE].
[30] I. Tews, J. M. Lattimer, A. Ohnishi, and E. E. Kolomeitsev, The Astrophysical Journal **848**, 105 (2017).
[31] H. T. Cromartie *et al.*, Nat. Astron. **4**, 72 (2019), arXiv:1904.06759 [astro-ph.HE].
[32] K. Yagi and N. Yunes, Phys. Rept. **681**, 1 (2017), arXiv:1608.02582 [gr-qc].
[33] J. Dong, W. Zuo, J. Gu, and U. Lombardo, Phys. Rev. C **85**, 034308 (2012).
[34] W.-J. Xie and B.-A. Li, Astrophys. J. **883**, 174 (2019), arXiv:1907.10741 [astro-ph.HE].
[35] B. P. Abbott *et al.* (LIGO Scientific, Virgo), Phys. Rev. Lett. **121**, 161101 (2018), arXiv:1805.11581 [gr-qc].
[36] W.-J. Xie and B.-A. Li, Astrophys. J. **883**, 174 (2019), arXiv:1907.10741 [astro-ph.HE].